Proceedings of the 7th GACM Colloquium on Computational Mechanics
for Young Scientists from Academia and Industry
October 11-13, 2017 in Stuttgart, Germany

Phase field modelling of thermo-mechanically driven fracture processes in electronic control units

Fabian Welschinger[1]*

Micro Abstract
Phase field models for fracture allow shaping the reliability of engineering components in the early stage of the product development process. Epoxy-based molding compounds protect electronic control units from harsh environments. Once this protection fractures, the electronic system fails. Based on a fracture mechanical characterization of the mold material in the full temperature range, computations are performed demonstrating the predictive quality of the phase field model of fracture.

[1]Corporate Sector Research and Advance Engineering, Robert Bosch GmbH, Renningen, Germany
***Corresponding author**: fabian.welschinger@de.bosch.com

Introduction

Recently developed phase field models for fracture are powerful tools for modeling fracture processes in solids caused by complex loading scenarios. In an industrial environment, these models can be employed to shape the reliability of components in the early stage of the product development process. In the automotive industry, epoxy-based molding compounds are used to protect electronic control units from harsh environments. As illustrated in in Figure 1,

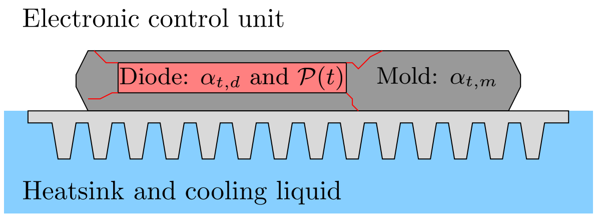

Figure 1. Electronic control unit. Thermal load might result in fracture of the encapsulating mold material.

active cycling of the diodes causes heat generation inside the electronic system resulting into inhomogeneous thermal strain and stress fields and potentially into fracture of the encapsulating material. In this case the entire electronic system loses its functionality which must be prevented.

1 Phase Field Modeling of Fracture

Current industrial research focuses on the application of a current phase field model of fracture [2, 3] extended towards thermally driven crack propagations as suggested by [5]. The algorithm is implemented into Abaqus using the user element inteface. Regarding a sequentially coupled thermo-mechanical simulation, the temperature field $\theta(\boldsymbol{x}, t)$ is obtained from a decoupled transient thermal simulation. In a subsequent mechanical analysis this temperature field is applied as a prescribed body load. As a consequence, a strong coupling of the temperature field with the mechanical response is present, whereas the fracture mechanical problem does not influence the thermal response. The solution algorithm can be summarized as follows:

i. *Initialization.* The displacement, fracture phase, history and temperature fields $\boldsymbol{u}_n$, d_n, $\mathcal{H}_n$ and θ_n at time t_n are known. Update prescribed loading $\bar{\boldsymbol{\gamma}}$, $\bar{\boldsymbol{u}}$, $\bar{\boldsymbol{t}}$ and $\bar{\theta}$ at time t.

ii. *Compute history.* Determine maximum crack driving function in deformation history

$$\mathcal{H}(\theta) = \begin{cases} \dfrac{\psi_0^+(\nabla_s \boldsymbol{u};\theta)}{G_c(\theta)/l} & \text{for} \quad \dfrac{\psi_0^+(\nabla_s \boldsymbol{u};\theta)}{G_c(\theta)/l} > \mathcal{H}_n \\ \mathcal{H}_n & \text{otherwise} \end{cases} \tag{1}$$

in the domain $\mathcal{B}$ and store it as a local history variable field.

iii. *Compute fracture phase field.* Determine the current fracture phase field d at frozen temperature field θ from the minimization problem of crack topology

$$d = \arg \inf_d \left[\int_{\mathcal{B}} \{ l\gamma(d, \nabla d) + \frac{\eta}{2\tau}(d - d_n)^2 + (1-d)^2\, \mathcal{H}(\theta) \}\, dV \right] \tag{2}$$

expressed in terms of the crack surface density function

$$\gamma(d, \nabla d) = \frac{1}{2l} d^2 + \frac{l}{2} |\nabla d|^2 . \tag{3}$$

iv. *Compute displacement field.* Determine the current displacement field $\boldsymbol{u}$ at frozen fracture phase and temperature fields d and θ from the minimization principle of elasticity

$$\boldsymbol{u} = \arg \inf_{\boldsymbol{u}} \left[\int_{\mathcal{B}} \{ \psi(\nabla_s \boldsymbol{u}, d; \theta) - \bar{\boldsymbol{\gamma}} \cdot \boldsymbol{u} \}\, dV - \int_{\partial \mathcal{B}_{\bar{t}}} \bar{\boldsymbol{t}} \cdot \boldsymbol{u}\, dA \right] \tag{4}$$

in terms of the damaged free energy density function

$$\psi(\nabla_s \boldsymbol{u}, d; \theta) = g(d)\, \psi_0^+(\nabla_s \boldsymbol{u}; \theta) + \psi_0^-(\nabla_s \boldsymbol{u}; \theta) \tag{5}$$

where the damage function $g(d) = (1-d)^2 + k$ is multiplied to positive portions only

$$\psi_0^\pm(\nabla_s \boldsymbol{u}; \theta) = \frac{\lambda}{2} \langle tr[\boldsymbol{\varepsilon}^e(\nabla_s \boldsymbol{u}; \theta)] \rangle_\pm^2 + \mu\, tr[\boldsymbol{\varepsilon}_\pm^e(\nabla_s \boldsymbol{u}; \theta)^2] \tag{6}$$

expressed in terms of the elastic stress producing strains $\boldsymbol{\varepsilon}^e(\nabla_s \boldsymbol{u}; \theta) = \nabla_s \boldsymbol{u} - \alpha_t \Delta\theta\, \mathbf{1}$. The decomposition of the total elastic strains into positive and negative contributions

$$\boldsymbol{\varepsilon}_\pm^e(\nabla_s \boldsymbol{u}; \theta) = \sum_{I=1}^{3} \langle \varepsilon^{eI} \rangle_\pm\, \boldsymbol{n}^I \otimes \boldsymbol{n}^I \tag{7}$$

bases on a spectral representation with eigenvalues ε^{eI} and principal directions $\boldsymbol{n}^I$.

The above solution algorithm is summarized in a very compact manner, for more detailed reading consult the publications cited above.

2 Fracture Mechanical Characterization with Compact Tension Test

The fracture mechanical tests are performed in the full temperature range of interest according to [1]. The resulting structural responses are illustrated in Figure 2. As expected the material exhibits the highest stiffness at low temperatures and increasing temperatures means a decreasing material stiffness. Due to increasing mobility of polymer chains at elevated temperature the ductility of the material increases with temperature. At $\theta = 150\,°C$ the amount of nonlinearity in the material response exceeds the permissible range for the evaluation of the critical energy release rate characterized by $F_{max}/F_{95\,\%} > 1.1$. In a moderate temperature range the critical energy release rate over temperature can be assumed to be constant below room temperature $G_{Ic}(\theta) = G_{Ic}^{RT}$ and to increase linearly with the temperature above room temperature $G_{Ic}(\theta) = G_{Ic}^{RT} + \Delta G_{Ic}(\theta - \theta_{RT})$ with $G_{Ic}^{RT} = 0.0841\ N/mm$ and $\Delta G_{Ic} = 0.0007\ N/(mm\,K)$.

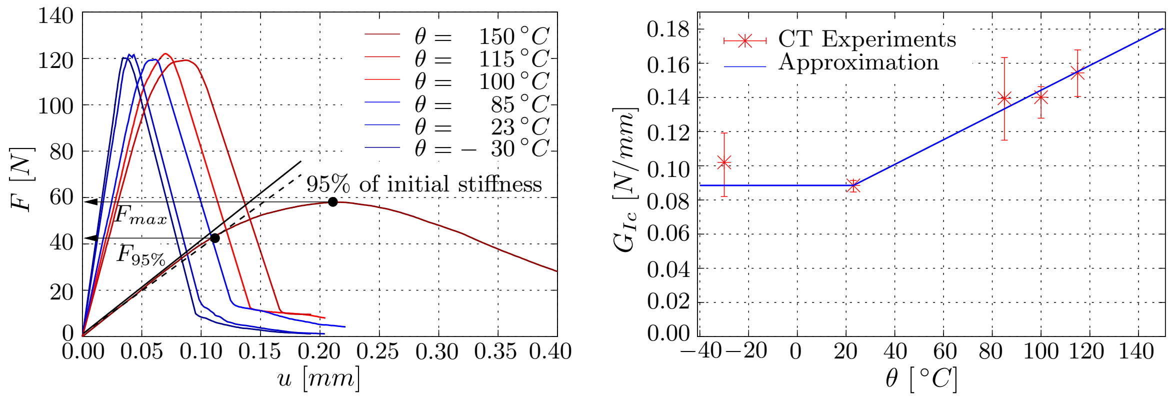

Figure 2. Compact tension test. Corrected load displacement curves according to [1] and resulting critical energy release rates over temperature. With increasing temperature the ductility of the material increases.

3 Validation of Simulation Methods

In what follows, the phase field model for fracture discussed in Section 1 in combination with the material parameters identified in Section 2 is validated based on two fundamental experiments.

3.1 Compact Tension Test

The first example used for validation of the simulation method is the compact tension test. In Figure 3 the experimentally determined load-deflection curves at temperatures of $\theta = 100\,°C$ and $\theta = 150\,°C$ are compared to numerical results obtained with a linear elastic fracture model realized with the extended finite element method and with the phase field model discussed previously. In the temperature range of interest, away from the glass transition temperature, the fracture mechanical behavior of the material can be predicted very nicely.

3.2 Compact Tension Shear Test

The last example discusses the influence of the mode mix ratio. As suggested by [4], the CTS specimens are loaded with different loading angles α. Figure 4 compares the experimentally and numerically obtained crack topologies for all variations of the loading angles. Figure 5 compares the ultimate force at rupture for different loading angles α and displays the crack topology for the loading angle $\alpha = 45.0\,°$. Both figures demonstrate very nicely the good prediction quality regarding the resulting crack pattern and the ultimate load at fracture. Compared to the fracture mechanical analysis using the extended finite element method the phase field approach yields values that are slightly closer to the experimental observations.

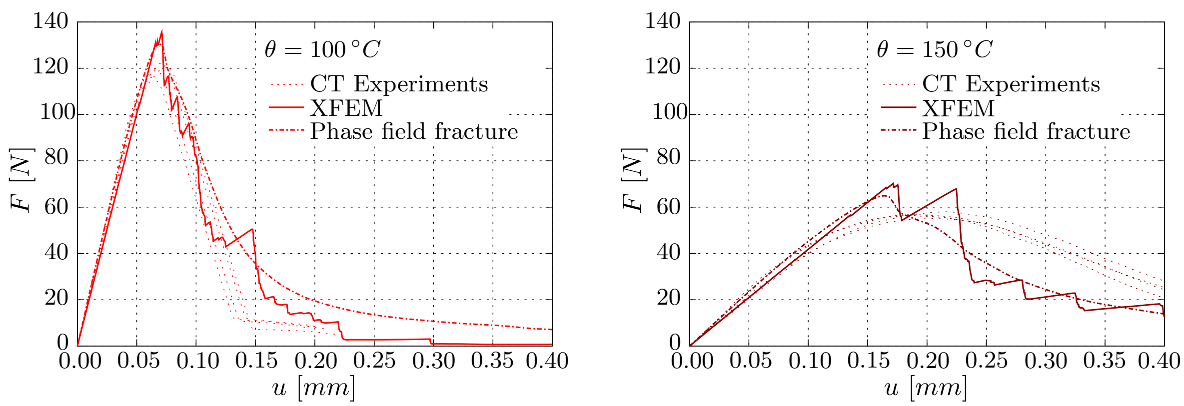

Figure 3. Validation with compact tension test. Good prediction quality at a temperatures of $\theta = 100\,°C$ and moderate accuracy at $\theta = 150\,°C$ due to increasing ductility around glass transition temperature.

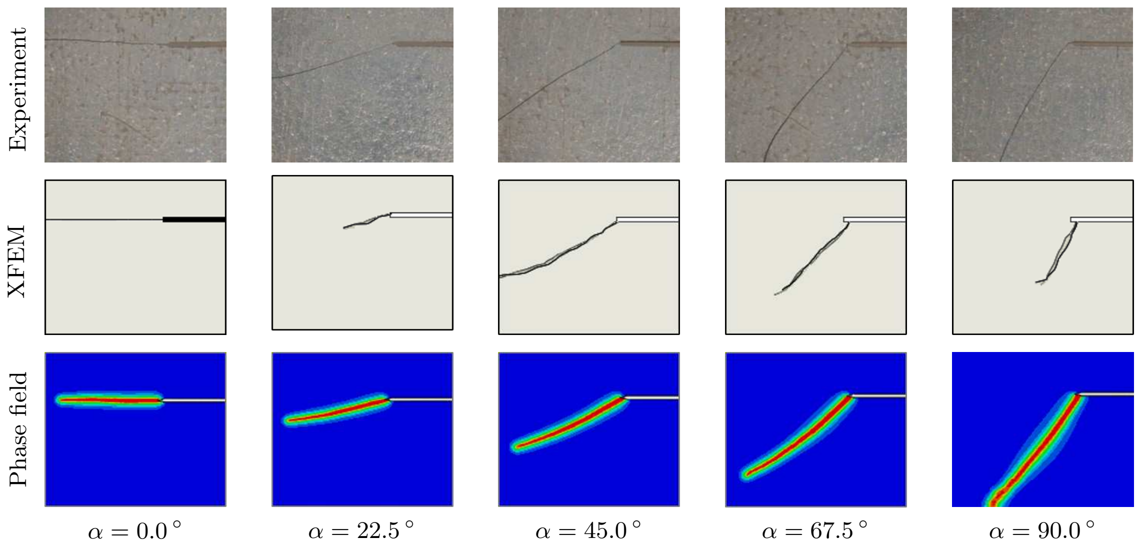

Figure 4. Validation with compact tension shear test. Good prediction quality regarding crack path.

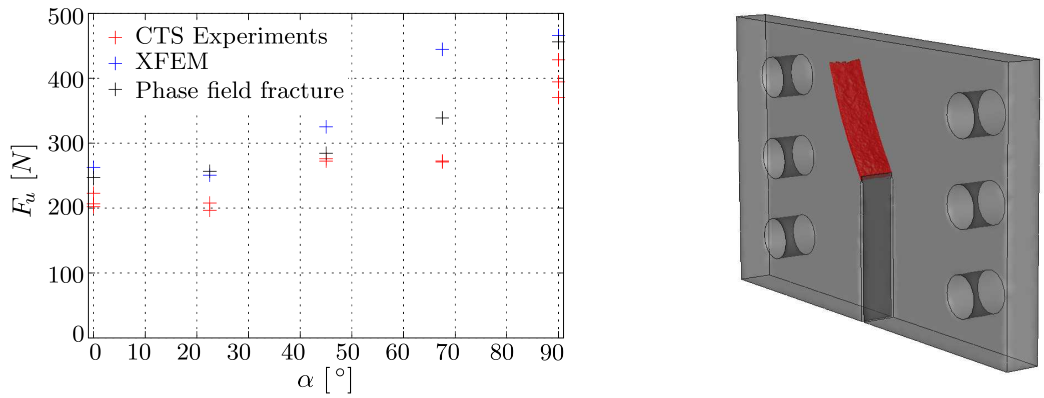

Figure 5. Validation with compact tension shear test. Good estimates for ultimate load at failure.

Conclusions

The main ingredients of a phase field model for thermally induced fracture and the required fracture mechanical characterization have been discussed. A comparison of numerical simulations and real experiments document an excellent prediction quality in the full temperature range.

References

[1] *ISO 13586: Plastics – Determination of fracture toughness (G_{Ic} and K_{Ic}) – Linear elastic fracture mechanics (LEFM) approach*. ISO 2000 International Standard, 2000.

[2] C. Miehe, M. Hofacker, and F. Welschinger. A phase field model for rate-independent crack propagation: Robust algorithmic implementation based on operator splits. *Computer Methods in Applied Mechanics and Engineering*, Vol. 199: p. 2765–2778, 2010.

[3] C. Miehe, F. Welschinger, and M. Hofacker. Thermodynamically consistent phase-field models of fracture: Variational principles and multi-field FE implementations. *International Journal for Numerical Methods in Engineering*, Vol. 83: p. 1273–1311, 2010.

[4] H. A. Richard. Bruchvorhersagen bei überlagerter Normal- und Schubbeanspruchung von Rissen. *VDI Forschungsheft*, Vol. 631: p. 1–60, 1985.

[5] F. Welschinger and P. J. Gromala. Simulation methods for crack initiation and propagation in bulk mold material of electro mechanical components. *Electronic Components and Technology Conference (ECTC)*, IEEE 66th: p. 1039–1046, 2016.